

1 A high resolution simulation of groundwater and surface water over most of the continental US
2 with the integrated hydrologic model ParFlow v3

3
4 Reed M Maxwell^{1*}, Laura E Condon¹, Stefan J Kollet²

5 ¹*Hydrologic Science and Engineering Program, Integrated GroundWater Modeling Center, Department*
6 *of Geology and Geological Engineering, Colorado School of Mines, Golden, Colorado, USA*

7 ²*Centre for High-Performance Scientific Computing in Terrestrial Systems, Institute for Bio- and*
8 *Geosciences, Agrosphere (IBG-3), Research Centre Jülich, Jülich, DE*

9
10 *correspondence to: Reed M Maxwell, rmaxwell@mines.edu

11
12 **Abstract**

13 Interactions between surface and groundwater systems are well-established theoretically and
14 observationally. While numerical models that solve both surface and subsurface flow equations
15 in a single framework (matrix) are increasingly being applied, computational limitations have
16 restricted their use to local and regional studies. Regional or watershed-scale simulations have
17 been effective tools in understanding hydrologic processes, however there are still many
18 questions, such as the adaptation of water resources to anthropogenic stressors and climate
19 variability, that need to be answered across large spatial extents at high resolution. In response
20 to this ‘grand challenge’ in hydrology, we present the results of a parallel, integrated hydrologic
21 model simulating surface and subsurface flow at high spatial resolution (1km) over much of
22 continental North America (~6,300,000 or 6.3M km²). These simulations provide integrated
23 predictions of hydrologic states and fluxes, namely water table depth and streamflow, at very
24 large scale and high resolution. The physics-based modeling approach used here requires limited
25 parameterizations and relies only on more fundamental inputs, such as topography,
26 hydrogeologic properties and climate forcing. Results are compared to observations and provide
27 mechanistic insight into hydrologic process interaction. This study demonstrates both the
28 feasibility of continental scale integrated models and their utility for improving our
29 understanding of large-scale hydrologic systems; the combination of high resolution and large
30 spatial extent facilitates novel analysis of scaling relationships using model outputs.

31 **Introduction**

32 There is growing evidence of feedbacks between groundwater, surface water and soil
33 moisture that moderate land-atmospheric energy exchanges, and impact weather and climate
34 (Maxwell et al. 2007; Anyah et al. 2008; Kollet and Maxwell 2008; Maxwell and Kollet 2008;
35 Jiang et al. 2009; Rihani et al. 2010; Maxwell et al. 2011; Williams and Maxwell 2011; Condon
36 et al. 2013; Taylor et al. 2013). While local observations and remote sensing can now detect
37 changes in the hydrologic cycle from small to very large spatial scales (e.g. Rodell et al. 2009),
38 theoretical approaches to connect and scale hydrologic states and fluxes from point
39 measurements to the continental scales are incomplete. In this work, we present integrated
40 modeling as one means to bridge this gap via numerical experiments.

41 Though introduced as a concept in the literature almost half a century ago (Freeze and
42 Harlan 1969), integrated hydrologic models that solve the surface and subsurface systems
43 simultaneously have only been a reality for about a decade (VanderKwaak and Loague 2001;
44 Jones et al. 2006; Kollet and Maxwell 2006). Since their implementation, integrated hydrologic
45 models have been successfully applied to a wide range of watershed-scale studies (see Table 1 in
46 Maxwell et al. 2014) successfully capturing observed surface and subsurface behavior (Qu and
47 Duffy 2007; Jones et al. 2008; Sudicky et al. 2008; Camporese et al. 2010; Shi et al. 2013),
48 diagnosing stream-aquifer and land-energy interactions (Maxwell et al. 2007; Kollet and
49 Maxwell 2008; Rihani et al. 2010; Condon et al. 2013; Camporese et al. 2014), and building our
50 understanding of the propagation of perturbations such as land-cover and anthropogenic climate
51 change throughout the hydrologic system (Maxwell and Kollet 2008; Goderniaux et al. 2009;
52 Sulis et al. 2012; Mikkelsen et al. 2013).

53 Prior to this work, computational demands and data constraints have limited the
54 application of integrated models to regional domains. Advances in parallel solution techniques,
55 numerical solvers, supercomputer hardware, and additional data sources have only recently made
56 large-scale, high-resolution simulation of the terrestrial hydrologic cycle technically feasible
57 (Kollet et al. 2010; Maxwell 2013). As such, existing large scale studies of the subsurface have
58 focused on modeling groundwater independently (Fan et al. 2007; Miguez-Macho et al. 2007;
59 Fan et al. 2013) and classifying behavior with analytical functions (Gleeson et al. 2011).
60 Similarly, continental scale modeling of surface water has utilized tools with simplified
61 groundwater systems that do not capture lateral groundwater flow and model catchments as
62 isolated systems (Maurer et al. 2002; Döll et al. 2012; Xia et al. 2012), despite the fact that lateral
63 flow of groundwater has been shown to be important across scales (Krakauer et al. 2014). While
64 much has been learned from previous studies, the focus on isolated components within what we
65 know to be an interconnected hydrologic system is a limitation that can only be addressed with
66 an integrated approach.

67 The importance of groundwater surface water interactions in governing scaling behavior
68 of surface and subsurface flow from headwaters to the continent has yet to be fully characterized.
69 Indeed, one of the purposes for building an integrated model is to better understand and predict
70 the nature of hydrologic connections across scales and throughout a wide array of physical and
71 climate settings. Arguably, this is not possible utilizing observations, because of data scarcity
72 and the challenges observing 3D groundwater flow across a wide range of scales. For example,
73 the scaling behavior of river networks is well known (Rodriguez-Iturbe and Rinaldo 2001), yet
74 open questions remain about the quantity, movement, travel time, and spatial and temporal
75 scaling of groundwater and surface water at the continental scale. Exchange processes and flow

76 near the land surface are strongly non-linear, and heterogeneity in hydraulic properties exist at all
77 spatial scales. As such, a formal framework for connecting scales in hydrology (Wood 2009)
78 needs to account for changes in surface water and groundwater flow from the headwaters to the
79 mouth of continental river basins. We propose that integrated, physics-based hydrologic models
80 are a tool for providing this understanding, solving fundamental non-linear flow equations at
81 high spatial resolution while *numerically* scaling these physical processes up to a large spatial
82 extent i.e. the continent.

83 In this study, we simulate surface and subsurface flow at high spatial resolution (1km)
84 over much of continental North America (6.3M km²), which is itself considered a grand
85 challenge in hydrology (e.g. Wood et al. 2011; Gleeson and Cardiff 2014). The domain is
86 constructed entirely of available datasets including topography, soil texture and hydrogeology
87 This simulation solves surface and subsurface flow simultaneously and takes full advantage of
88 massively parallel, high-performance computing. The results presented here should be viewed as
89 a sophisticated numerical experiment, designed to diagnose physical behavior and evaluate
90 scaling relationships. While this is not a calibrated model that is intended to match observations
91 perfectly, we do verify that behavior is realistic by comparing to both groundwater and surface
92 water observations.

93 The paper is organized as follows: first a brief description of the model equations are
94 provided including a description of the input variables and observational datasets used for model
95 comparison; next model simulations are compared to observations in a number of ways, and then
96 used to understand hydrodynamic characteristics and to describe scaling.

97
98

99 **Methods**

100 The model was constructed using the integrated simulation platform ParFlow (Ashby and
101 Falgout 1996; Jones and Woodward 2001; Kollet and Maxwell 2006) utilizing the terrain
102 following grid capability (Maxwell 2013). ParFlow is a physically based model that solves both
103 the surface and subsurface systems simultaneously. In the subsurface ParFlow solves the mixed
104 form of Richards' equation for variably saturated flow (Richards 1931) in three spatial
105 dimensions given as:

$$106 \quad S_s S_w(h) \frac{\partial h}{\partial t} + \phi S_w(h) \frac{\partial S_w(h)}{\partial t} = \nabla \cdot \mathbf{q} + q_r(x, z) \quad (1)$$

107 where the flux term \mathbf{q} [LT^{-1}] is based on Darcy's law:

$$108 \quad \mathbf{q} = -\mathbf{K}_s(\mathbf{x}) k_r(h) [\nabla(h + z) \cos \theta_x + \sin \theta_x] \quad (2)$$

109 In these expressions, h is the pressure head [L]; z is the elevation with the z -axis specified as
110 upward [L]; $\mathbf{K}_s(\mathbf{x})$ is the saturated hydraulic conductivity tensor [LT^{-1}]; k_r is the relative
111 permeability [-]; S_s is the specific storage [L^{-1}]; ϕ is the porosity [-]; S_w is the relative saturation [-
112]; q_r is a general source/sink term that represents transpiration, wells, and other fluxes [T^{-1}]; and
113 θ [-] is the local angle of slope, in the x and y directions and may be written as
114 $\theta_x = \tan^{-1} S_x$ and $\theta_y = \tan^{-1} S_y$. Note that we assume that density and viscosity are both
115 constant, although ParFlow can simulate density and viscosity-dependent flow (Kollet et al.
116 2009). The van Genuchten (1980) relationships are used to describe the relative saturation and
117 permeability functions ($S_w(h)$ and $k_r(h)$ respectively). These functions are highly nonlinear and
118 characterize changes in saturation and permeability with pressure.

119 Overland flow is represented in ParFlow by the two-dimensional kinematic wave
120 equation resulting from application of continuity conditions for pressure and flux (Kollet and
121 Maxwell 2006):

122 $\mathbf{k} \cdot (-\mathbf{K}_s(\mathbf{x})k_r(h) \cdot \nabla(h+z)) = \frac{\partial \|h,0\|}{\partial t} - \nabla \cdot \|h,0\| \mathbf{v}_{sw} + \lambda q_r(\mathbf{x})$ (3)

123 In this equation \mathbf{v}_{sw} is the two-dimensional, depth-averaged surface water velocity [LT^{-1}] given
 124 by Manning's equation; h is the surface ponding depth [L] the same h as is shown in Equation 1.
 125 Note that $\|h,0\|$ indicates the greater value of the two quantities in Equation 3. This means that
 126 if $h < 0$ the left hand side of this equation represents vertical fluxes (e.g. in/exfiltration) across
 127 the land surface boundary and is equal to $q_r(\mathbf{x})$ and a general source/sink (e.g. rainfall, ET) rate
 128 [LT^{-1}] with λ being a constant equal to the inverse of the vertical grid spacing [L^{-1}]. This term is
 129 then entirely equivalent to the source/sink term shown in Equation 1 at the ground surface where
 130 \mathbf{k} is the unit vector in the vertical, again defining positive upward coordinates. If $h > 0$ then the
 131 terms on the right hand side of Equation 3 are active water that is routed according to surface
 132 topography (Kollet and Maxwell 2006).

133 The nonlinear, coupled equations of surface and subsurface flow presented above are
 134 solved in a fully-implicit manner using a parallel Newton-Krylov approach (Jones and
 135 Woodward 2001; Kollet and Maxwell 2006; Maxwell 2013). Utilizing a globally-implicit
 136 solution allows for interactions between the surface and subsurface flow system to be explicitly
 137 resolved. While this yields a very challenging computational problem, ParFlow is able to solve
 138 large complex systems by utilizing a multigrid preconditioner (Osei-Kuffuor et al. ; Ashby and
 139 Falgout 1996) and taking advantage of highly scaled parallel efficiency out to more than $1.6 \times$
 140 10^4 processors (Kollet et al. 2010; Maxwell 2013).

141 Physically this means that ParFlow solves saturated subsurface flow (i.e. groundwater),
 142 unsaturated subsurface flow (i.e. the vadose zone) and surface flow (i.e. streamflow) in a
 143 continuum approach within a single matrix. Thus, complete non-linear interactions between all
 144 system components are simulated without *a priori* specification of what types of flow occur in

145 any given portion of the grid. Streams form purely based on hydrodynamic principles governed
146 by recharge, topography, hydraulic conductivity and flow parameters, when water is ponded due
147 to either excess infiltration (surface fluxes exceed the infiltration capacity, e.g. Horton 1933) or
148 excess saturation (subsurface exfiltration to the surface system, e.g. Dunne 1983) for further
149 discussion see Kirkby (1988) and Beven (2004) for example. Groundwater converges in
150 topographic depressions and unsaturated zones may be shallow or deep depending upon recharge
151 and lateral flows.

152 The physically based approach used by ParFlow is similar to other integrated hydrologic
153 models such as Hydrogeosphere (Therrien et al. 2012), PIHM (Kumar et al. 2009) and CATHY
154 (Camporese et al. 2010). This is a distinct contrast to more conceptually-based models that may
155 not simulate lateral groundwater flow or simplify the solution of surface and subsurface flow by
156 defining regions of groundwater or the stream-network prior to the simulation. In such models,
157 groundwater surface water interactions are often captured as one-way exchanges (i.e. surface
158 water loss to groundwater) or parameterized with simple relationships (i.e. functional
159 relationships to impose the relationship between stream head and baseflow). The integrated
160 approach used by ParFlow eliminates the need for such assumptions and allows the
161 interconnected groundwater surface water systems to evolve dynamically based only on the
162 governing equations and the properties of the physical system. The approach used here requires
163 robust numerical solvers (Maxwell 2013; Osei-Kuffuor et al. 2014) and exploits high-
164 performance computing (Kollet et al. 2010) to achieve high resolution, large extent simulations.

165

166

167

168 **Domain Setup**

169 In this study, the model and numerical experiment was directed at the Continental US
170 (CONUS) using the terrain following grid framework (Maxwell 2013) for a total thickness of
171 102m over 5 model layers. The model was implemented with a lateral resolution of 1km with
172 $n_x=3342$, $n_y=1888$ and five vertical layers with 0.1, 0.3, 0.6, 1.0 and 100m discretization for a
173 total model dimensions of 3,342 by 1,888 by 0.102 km and 31,548,480 total compute cells. The
174 model domain and input data sets are shown in Figure 1. All model inputs were re-projected to
175 have an equal cell-size of 1x1km as shown in Figure 1. Topographic slopes (S_x and S_y) were
176 calculated from the Hydrosheds digital elevation model (Figure 1b) and were processed using the
177 r.watershed package in the GRASS GIS platform. Surface roughness values were constant 10^{-5}
178 [$\text{h m}^{-1/3}$] outside of the channels and varied within the channel as a function of average
179 watershed slope. Over the top 2m of the domain, hydraulic properties from soil texture
180 information of SSURGO were applied and soil properties were obtained from Schaap and Leij
181 (1998) . Note that two sets of soil categories were available. The upper horizon was applied over
182 the top 1m (the top three model layers) and the bottom one over the next 1m (the fourth model
183 layer). Figures 1a and c show the top and bottom soil layers of the model. The deeper subsurface
184 (i.e. below 2m) was constructed from a global permeability map developed by Gleeson et al.
185 (2011). These values (Gleeson et al. 2011) were adjusted to reduce variance (Condon and
186 Maxwell 2013; Condon and Maxwell 2014) and to reflect changes in topography using the e-
187 folding relationship empirically-derived in (Fan et al. 2007): $\alpha = e^{-\frac{50}{f}}$ where $f = \frac{a}{\left(1+b*\sqrt{S_x^2+S_y^2}\right)}$
188 . For this analysis $a=20$, $b=125$ and the value of 50 [m] was chosen to reflect the midpoint of the
189 deeper geologic layer in the model. Larger values of α reduced the hydraulic conductivity
190 categorically, that is by decreasing the hydraulic conductivity indicator values in regions of

191 steeper slope. Figure 1e maps the final conductivity values used for simulation. Note that this
192 complex subsurface dataset is assembled from many sources and is subject to uncertainty. As
193 such there are breaks across dataset boundaries, commonly at State or Province and International
194 political delineations. The fidelity and resolution of the source information used to formulate this
195 dataset also changes across these boundaries yielding some interfaces in property values.

196 All input datasets are a work in progress and should be continually improved. However,
197 we feel it is important to continue numerical experiments with the data that is currently available,
198 while keeping in mind the limitations associated with every model input. Shortcomings in
199 hydrogeological data sets reflect the lack of detailed unified hydrogeological information that
200 can be applied in high resolution continental models. This constitutes a significant source of
201 uncertainty, which needs to be assessed, quantified and ultimately reduced in order to arrive at
202 precise predictions. Still, it should be noted that the purpose of this work is to demonstrate the
203 feasibility of integrated modeling to explicitly represent processes across many scales of spatial
204 variability. By focusing on large-scale behaviors and relationships we limit the impact uncertain
205 inputs.

206 No-flow boundary conditions were imposed on all sides of the model except the land
207 surface, where the free-surface overland flow boundary condition was applied. For the surface
208 flux, a Precipitation-Evapotranspiration (P-E, or potential recharge) product was derived from a
209 combination of precipitation and model-simulated evaporation and transpiration fluxes for a
210 product very similar to Maurer et al. (2002), shown in Figure 1d. The model was initialized dry
211 and the P-E forcing was applied continuously at the land surface until the balance of water
212 (difference between total outflow and P-E) was less than 3% of storage. For all simulations a

213 nonlinear tolerance of 10^{-5} and a linear tolerance of 10^{-10} were used to ensure proper model
214 convergence.

215 While this study employs state of the art modeling techniques, it is important to note that
216 the numerical simulation of this problem is far from being trivial. Simulations were split over
217 128 divisions in the x -direction and 128 in the y -direction and run on 16,384 compute-cores of an
218 IBM BG/Q supercomputer (JUQUEEN) located at the Jülich Supercomputing Centre, Germany.
219 These processor splits resulted in approximately 2,000 unknowns per compute core; a relatively
220 small number, yet ParFlow's scaling was still good (better than 60% efficiency) due to the non-
221 symmetric preconditioner used (Maxwell 2013). The reason for this is the special architecture of
222 JUQUEEN with only 256MB of memory per core and relatively slow clock rate. Additionally,
223 code performance was improved using efficient preconditioning of the linear system (Osei-
224 Kuffuor et al.). The steady-state flow field was accomplished over several steps. Artificial
225 dampening was applied to the overland flow equations early in the simulation during water table
226 equilibration. Dampening was subsequently decreased and removed entirely as simulation time
227 progressed. Large time steps (10,000h) were used initially and were decreased (to 1h) as the
228 stream network formed and overland flow became more pronounced with reduced dampening.
229 The entire simulation utilized approximately 2.5M core hours of compute time, which resulted in
230 less than 1 week of wall-clock time (approximately 150 hours) given the large core counts and
231 batch submission process.

232 Model results were checked for plausibility against available observations of streamflow
233 and hydraulic head (the sum of pressure head and gravitational potential). Observed streamflow
234 values were extracted from a spatial dataset of current and historical U.S. Geological Survey
235 (USGS) stream gages mapped to the National Hydrography Dataset (NHD) (Stewart et al.,

236 2006). The entire dataset includes roughly 23,000 stations, of which just over half (13,567) fall
237 within the CONUS domain. For each station, the dataset includes location, drainage area,
238 sampling time period and flow characteristics including minimum, maximum, mean and a range
239 of percentiles (1, 5, 10, 20, 25, 50, 75, 80, 90, 95, 99) compiled from the USGS gage
240 records. For comparison, stations without a reported drainage area, stations not located on or
241 adjacent to a river cell in ParFlow, and stations whose drainage area were not within twenty
242 percent of the calculated ParFlow drainage area were filtered out. This resulted in 4,736 stations
243 for comparison. The 50th percentile values for these stations are shown in Figure 2a. Note that
244 these observations are not naturalized, i.e. no attempt is made to remove dams and diversions
245 along these streams and rivers, however some of these effects will be minimized given the longer
246 temporal averages. Hydraulic head observations of groundwater at more than 160,000 locations
247 were assembled by Fan et al. (Fan et al. 2007; Fan et al. 2013). Figure 2b plots the
248 corresponding water table depth at each location calculated as the difference between elevation
249 and hydraulic head. Note that these observations include groundwater pumping (most wells are
250 drilled for extraction rather than purely observation).

251

252 **Results and Discussion**

253 Figures 3 and 4 plot simulated streamflow and water table depth, respectively, over much
254 of continental North America, both on a log scale for flow (Figure 3) and water table depth
255 (Figure 4). Figure 3 shows a complex stream network with flow rates spanning many orders of
256 magnitude. Surface flows originate in the headwaters (or recharge zones) creating tributaries that
257 join to form the major river systems in North America. Note, as discussed previously that the
258 locations for flowing streams are not enforced in ParFlow but form due to ponded water at the

259 surface (i.e. values of $h > 0$ in the top layer of the model in Equations 1-3). Overland flow is
260 promoted both by topographic convergence, and surface and subsurface flux; however, with this
261 formulation there is no requirement that all potential streams support flow. Thus, the model
262 captures the generation of the complete stream network without specifying the presence and
263 location of rivers in advance, but rather by allowing channelized flow to evolve as a result of
264 explicitly simulated non-linear physical processes.

265 The insets in Figure 3 demonstrate multiscale detail ranging from the continental river
266 systems to the first-order headwaters. In Figure 4, water table depth also varies over five orders
267 of magnitude. Whereas aridity drives large-scale differences in water table depth (Figure 1d), at
268 smaller scales, lateral surface and subsurface flow processes clearly dominate recharge and
269 subsurface heterogeneity (see insets to Figure 4). Water tables are deeper in the more arid
270 western regions, and shallower in the more humid eastern regions of the model. However, areas
271 of shallow water table exist along arid river channels and water table depths greater than 10m
272 exist in more humid regions. Note that this is a pre-development simulation, thus, results do not
273 include any anthropogenic water management features such as groundwater pumping, surface
274 water reservoirs, irrigation or urbanization—all of which are present in the observations. Many
275 of these anthropogenic impacts have been implemented into the ParFlow modeling framework
276 (Ferguson and Maxwell 2011; Condon and Maxwell 2013; Condon and Maxwell 2014). While
277 anthropogenic impacts are clearly influential on water resources, a baseline simulation allows for
278 a comparison between the altered and unaltered systems in future.

279 Next we compare the results of the numerical experiment to observations. As noted
280 previously, this is not a calibrated model. Therefore, the purpose of these comparisons is to
281 provide a plausibility check of model behavior and physical processes. Figure 5 plots observed

282 and simulated hydraulic head and streamflow for the dataset shown in Figure 2. Hydraulic head
283 (Figure 5a) is plotted (as opposed to water table depth) as it is the motivating force for lateral
284 flow in the simulation; it includes both the topography and pressure influences on the final
285 solution. We see a very close agreement between observations and model simulations, though
286 given the large range in hydraulic heads the goodness of fit may be somewhat driven by the
287 underlying topography. Additional metrics and comparisons are explored below. Simulated
288 streamflow (Figure 5b) also agrees closely with observations. There is some bias, particularly
289 for smaller flows (which we emphasize by plotting in log scale), which also exhibit more scatter
290 than larger flows, and are likely due to the 1km grid resolution employed here. Larger flows are
291 more integrated measures of the system and might be less sensitive to resolution or local
292 heterogeneity in model parameters. We see this when linear least squared statistics are computed
293 where the R^2 value increases to 0.8.

294 Figure 6 plots histograms of predicted and observed water table depth (a), hydraulic head
295 (b), median (50th percentile) flow and 75th percentile flows (c-d). The hydraulic head shows
296 good agreement between simulated and observed (Figure 6b). While hydraulic head is the
297 motivation for lateral flow and has been used in prior comparisons (e.g. Fan et al 2007) both
298 observed and simulated values are highly dependent on the local elevation. Figure 6a plots the
299 water table depth below ground surface, or the difference between local elevation and
300 groundwater. Here we see the simulated water table depths are shallower than the observed,
301 something observed in prior simulations of large-scale water table depth (Fan et al 2013). The
302 observed water tables may include anthropogenic impacts, namely groundwater pumping, while
303 the model simulations do not and this is a likely cause for this difference. Also, because
304 groundwater wells are usually installed for extraction purposes there is no guarantee that the

305 groundwater observations are an unbiased sample of the system as a whole. Figure 6c plots the
306 steady-state derived flow values compared to median observed flow values and Figure 6d plots
307 these same steady-state simulated flows compared to the 75th percentile of the observed transient
308 flow at each station. While the ParFlow model provides a robust representation of runoff
309 generation processes, the steady-state simulations average event flows. We see the model
310 predicts greater flow than the 50th percentile observed flows (Figure 6c) and good agreement
311 between the model simulations and the 75th percentile observed flows (Figure 6d). This
312 indicates a potentially wet bias in the forcing, which might also explain the shallower water table
313 depths.

314 Figures 7 and 8 compare observed and simulated flows and water table depths for each of
315 the major basin encompassed by the model. Water tables are generally predicted to be shallower
316 in the model than observations with the exception of the Upper and Lower Colorado which
317 demonstrate better agreement between model simulations and observations than other basins.
318 These histograms agree with a visual inspection of Figures 2b and 4 which also indicate deeper
319 observed water tables. Figure 8 indicates that simulated histograms of streamflow also predict
320 more flow than the observations. This might indicate that the P-E forcing is too wet. However,
321 a comparison of streamflow for the Colorado Watershed, where water table depths agree (Figure
322 8 e and g) and flows are overpredicted (Figure 7 e and g), indicates a more complex set of
323 interactions than basic water balance driven by forcing.

324 To better diagnose model processes, model inputs are compared with model simulation
325 outputs over example regions chosen to isolate the impact of topographic slope, forcing and
326 hydraulic conductivity on subsurface-surface water hydrodynamics. We do this as a check to see
327 if and how this numerical experiment compares to real observations. It is important to use a

328 range of measures of success that might be different from that used in a model calibration where
329 inadequacies in model parameters and process might be muted while tuning the model to better
330 match observations. Figure 9 juxtaposes slope, potential recharge, surface flow, water table
331 depth, hydraulic conductivity and a satellite image composite also at 1km resolution (the NASA
332 Blue Marble image, (Justice et al. 2002)) and facilitates a visual diagnosis of control by the three
333 primary model inputs. While the model was run to steady-state and ultimately all the potential
334 recharge has to exit the domain as discharge, the distribution and partitioning between
335 groundwater and streams depends on the slope and hydraulic conductivity. Likewise, while
336 topographic lows create the potential for flow convergence, it is not a model requirement that
337 these will develop into stream loci. Figure 9 demonstrates some of these relationships quite
338 clearly over a portion of the model that transitions from semi-arid to more humid conditions as
339 the North and South Platte River systems join the Missouri. As expected changes in slope yield
340 flow convergence, however, this figure also shows that as recharge increases from west to east
341 ($X > 1700$ km, panel c) the model generally predicts shallower water tables and greater stream
342 density (panels d and e, respectively). Conversely, in localized areas of decreased P-E (e.g. 700
343 $< Y < 900$ km specifically south of the Platte River) water tables increase and stream densities
344 decrease. The satellite image (panel f) shows increases in vegetation that correspond to
345 shallower water tables and increased stream density.

346 Hydraulic conductivity also has a significant impact on water table depth and stream
347 network density. In areas of greater recharge in the eastern portion of Figure 9c, regions with
348 larger hydraulic conductivity (panel b) show decreased stream network density and increased
349 water table depths. This is more clearly demonstrated in Figure 10 (a region in the upper
350 Missouri) where, except for the northeast corner, recharge is uniformly low. Slopes are also

351 generally low (panel a), yet hydraulic conductivities show a substantial increase due to a change
352 in datasets between state and country boundaries (panel b, $X > 1250\text{km}$, $Y > 1400\text{ km}$). The
353 relative increase in hydraulic conductivity decreases hydraulic gradients under steady state
354 conditions and generally increases water table depth, which in turn decreases stream network
355 density. This change in hydraulic conductivity yields a decrease in the formation of stream
356 networks resulting in an increase in water table depth. Thus, hydraulic conductivity has an
357 important role in partitioning moisture between surface and subsurface flow, also under steady-
358 state conditions. While mass balance requires that overall flow must be conserved, larger
359 conductivity values allow this flow to be maintained within the subsurface while lower
360 conductivities force the surface stream network to maintain this flow. In turn, stream networks
361 connect regions of varying hydrodynamic conditions and may result in locally infiltrating
362 conditions creating a losing-stream to recharge groundwater. This underscores the connection
363 between input variables and model predictions, an equal importance of hydraulic conductivity to
364 recharge in model states and the need to continually improve input datasets.

365 Finally, the connection between stream flow and drainage area is a classical scaling
366 relationship (Rodriguez-Iturbe and Rinaldo 2001), which usually takes the power law form
367 $Q=kA^n$, where Q is volumetric streamflow [L^3T^{-1}], A is the contributing upstream area [L^2] and k
368 [LT^{-1}] and n are empirical constants. While this relationship has been demonstrated for
369 individual basins and certain flow conditions (Rodriguez-Iturbe and Rinaldo 2001), generality
370 has not been established (Glaster 2009). Figure 11a plots simulated streamflow as a function of
371 associated drainage area on log-log axes, and Figure 11b plots the same variables for median
372 observed streamflow from more than 4,000 gaging stations. While no single functional
373 relationship is evident from this plot, there is a striking maximum limit of flow as a function of

374 drainage area with a continental scaling coefficient of $n = 0.84$. Both Figures 11a and b are
375 colored by aridity index (AI), the degree of dryness of a given location. Color gradients that
376 transition from blue (more humid) to red (more arid) show that humid basins fall along the
377 maximum flow-discharge line, while arid basins have less discharge and fall below this line. For
378 discharge observations (Figure 11b) the same behavior is observed, where more humid stations
379 fall along the $n=0.9$ line and more arid stations fall below this line. Essentially this means that in
380 humid locations, where water is not a limiting factor, streamflow scales most strongly with
381 topography and area. Conversely arid locations fall below this line because flow to streams is
382 limited by groundwater storage.

383

384 **Conclusions**

385 Here we present the results of an integrated, multiphysics-based hydrologic simulation
386 covering much of Continental North America at hyperresolution (1km). This numerical
387 experiment provides a consistent theoretical framework for the analysis of groundwater and
388 surface water interactions and scaling from the headwaters to continental scale (10^0 - 10^7 km²).
389 The framework exploits high performance computing to meet this grand challenge in hydrology
390 (Wood et al. 2011; Gleeson and Cardiff 2014; Bierkens et al. 2015). We demonstrate that
391 continental-scale, integrated hydrologic models are feasible and can reproduce observations and
392 the essential features of streamflow and groundwater. Results show that scaling of surface flow
393 is related to both drainage area and aridity. These results may be interrogated further to
394 understand the role of topography, subsurface properties and climate on groundwater table and
395 streamflow, and used as a platform to diagnose scaling behavior, e.g. surface flow from the
396 headwaters to the continent.

397 These presented results are a first-step in high resolution, integrated, continental-scale
398 simulation. We simulate an unaltered, or pre-development scenario of groundwater and surface
399 water flows under steady-state conditions. As such, the discussion focuses on the physical
400 controls of groundwater surface water interactions and scaling behavior; however there are
401 obvious limitations to this scenario and these simulations. Clearly reservoir management,
402 groundwater pumping, irrigation, diversion and urban expansion all shape modern hydrology.
403 Work has been undertaken to include these features within the ParFlow framework at smaller
404 scales (Ferguson and Maxwell 2011; Ferguson and Maxwell 2012; Condon and Maxwell 2013;
405 Condon and Maxwell 2014) and an important next step is to scale the impacts out to the
406 continent.

407 Additionally, the steady-state simulation does not take into consideration temporal
408 dynamics or complex land-surface processes, also important in determining the quantity and
409 fluxes of water. These limitations can all be addressed within the current modeling framework
410 but require transient simulations and additional computational resources. Model performance is
411 also limited by the quality of available input datasets. As noted throughout the discussion,
412 existing datasets are subject to uncertainty and are clearly imperfect. As improved subsurface
413 characterization becomes available, this information can be used to better inform models and
414 fully understand the propagation of uncertainty in these types of numerical experiments (e.g.
415 Maxwell and Kollet 2008; Kollet 2009). However, while the magnitudes of states and fluxes may
416 change with improved datasets, the overall trends and responses predicted here are not likely to
417 change within the confines of the numerical experiment. While there are always improvements
418 to be made, these simulations represent a critical first step in understanding coupled surface

419 subsurface hydrologic processes and scaling at continental scales resolving variances over four
420 for orders of spatial scales.

421 This study highlights the utility of high performance computing in addressing the grand
422 challenges in hydrological sciences and represents an important advancement in our
423 understanding of hydrologic scaling in continental river basins. By providing an integrated
424 model we open up a useful avenue of research to bridge physical processes across spatial scales
425 in a hydrodynamic, physics-based upscaling framework.

426

427 **Code Availability**

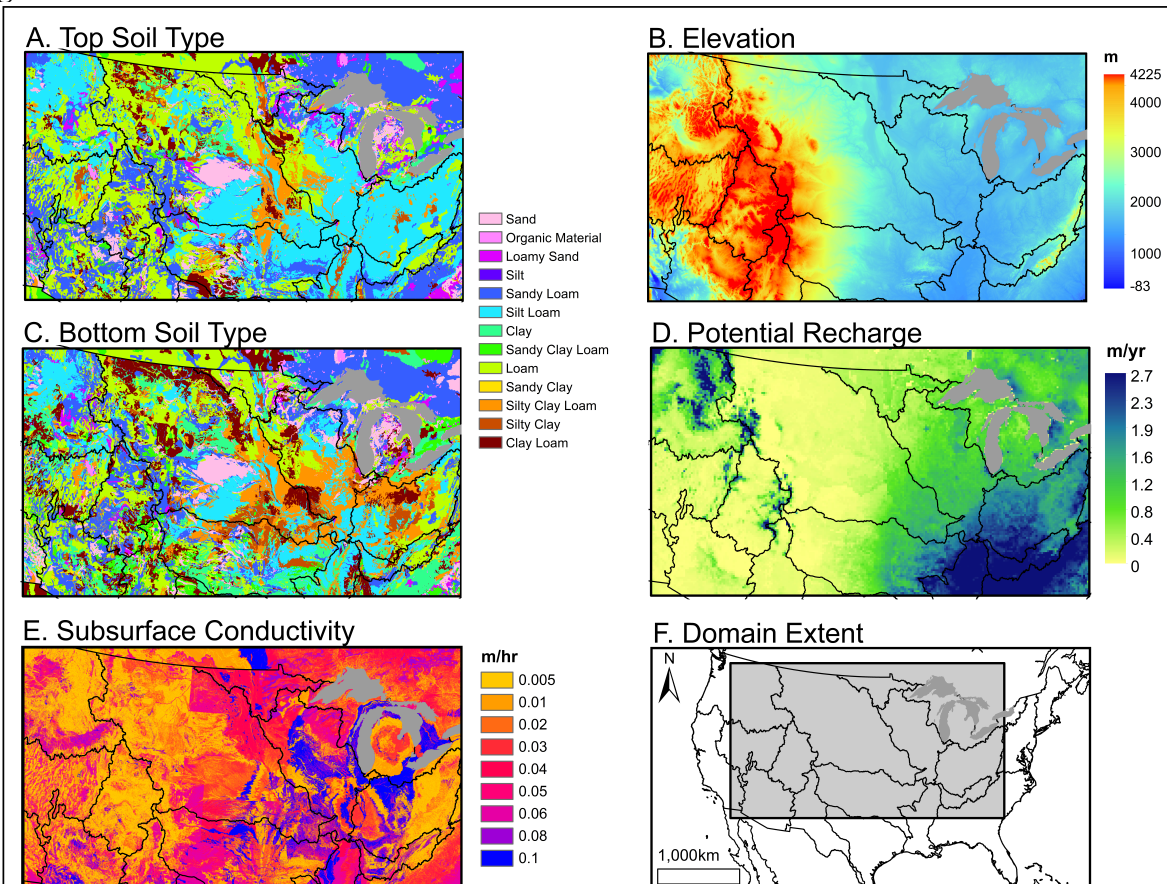
428 ParFlow is an open-source, modular, parallel integrated hydrologic platform freely available via
429 the GNU LPGL license agreement. ParFlow is developed by a community led by the Colorado
430 School of Mines and F-Z Jülich with contributors from a number of other institutions. Specific
431 versions of ParFlow are archived with complete documentation and may be downloaded¹ or
432 checked-out from a commercially hosted, free SVN repository; v3, r693 was the version used in
433 this study. The input data and simulations presented here will be made available and may be
434 obtained by contacting the lead author via email.

435

¹ http://inside.mines.edu/~rmaxwell/maxwell_software.shtml

436

437 **Figures**

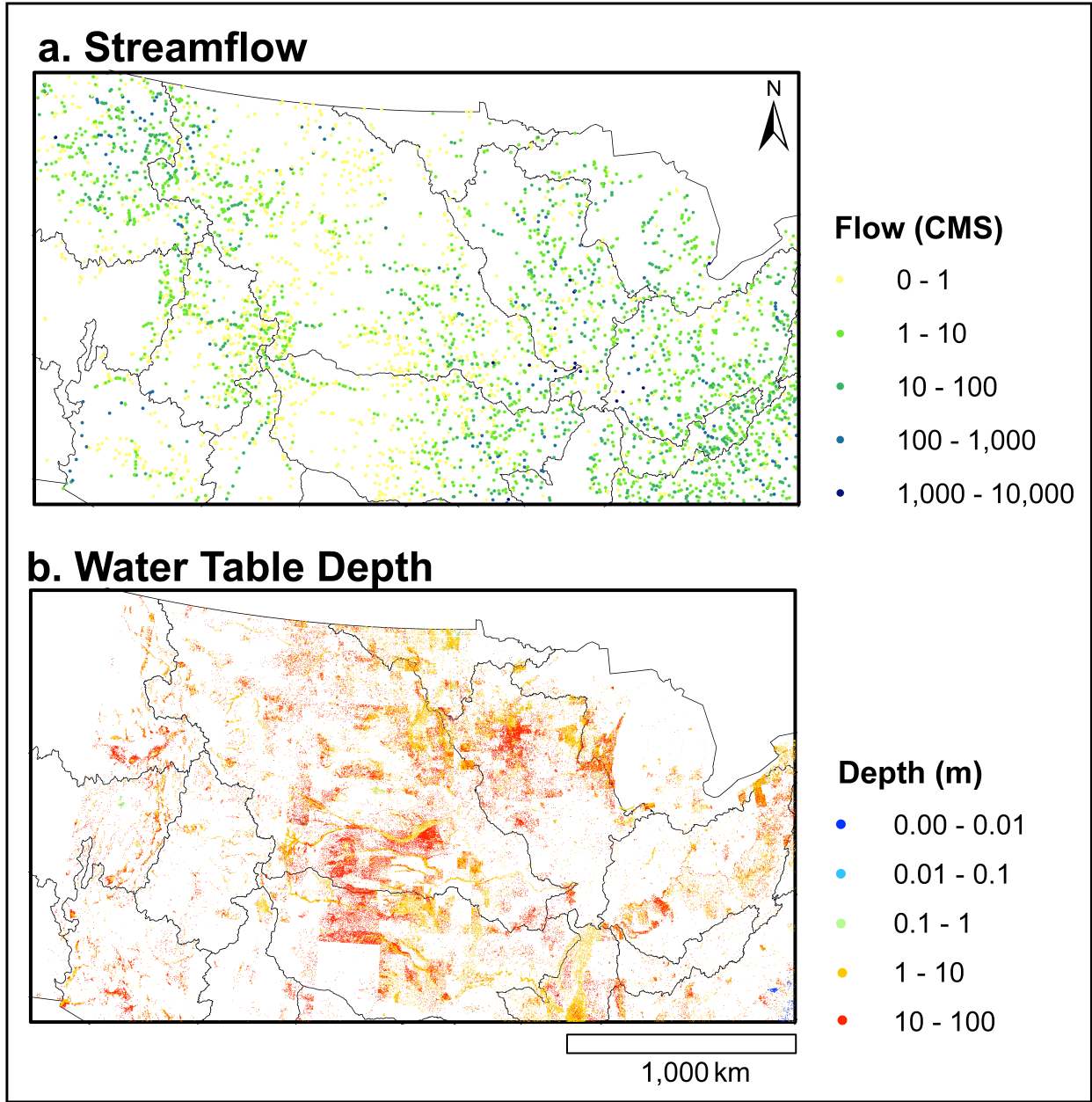


438

439 Figure 1. Maps of top soil type (a), elevation (masl) (b), bottom soil type (c), potential recharge,

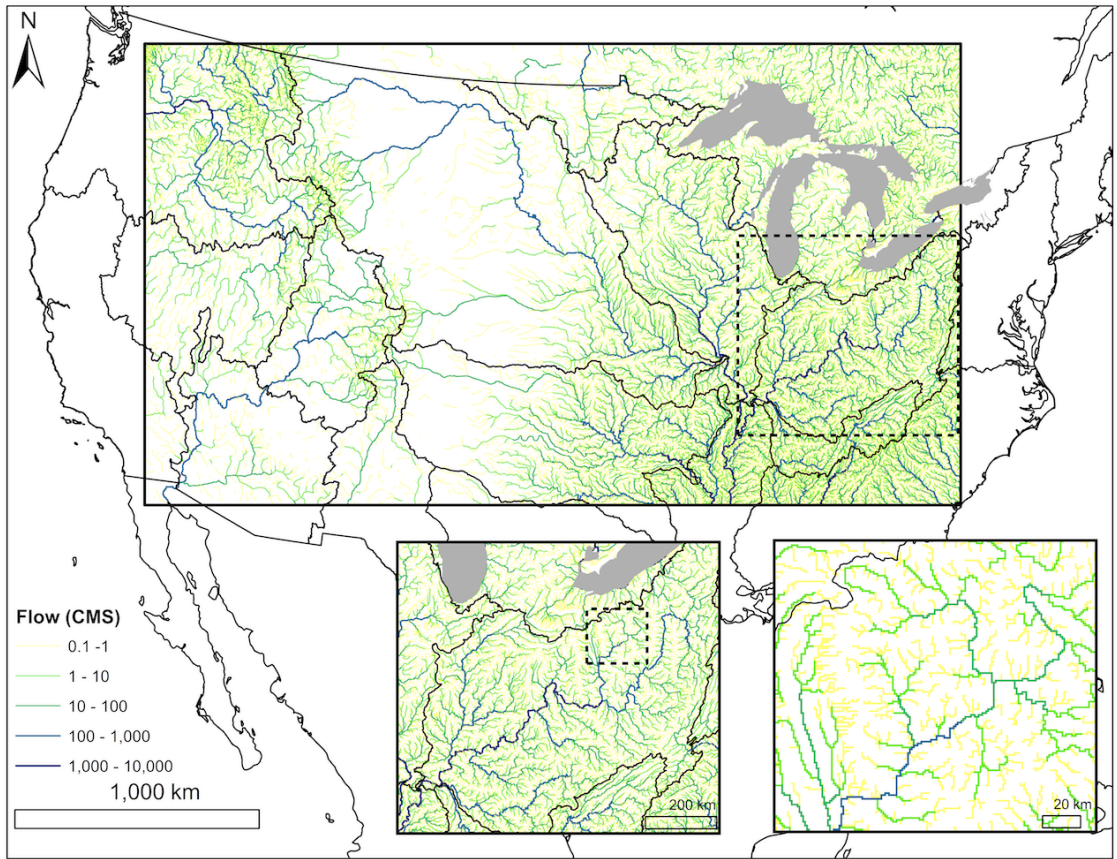
440 P-E, (m/y) (d), saturated hydraulic conductivity (m/h) (e) over the model domain (f).

441

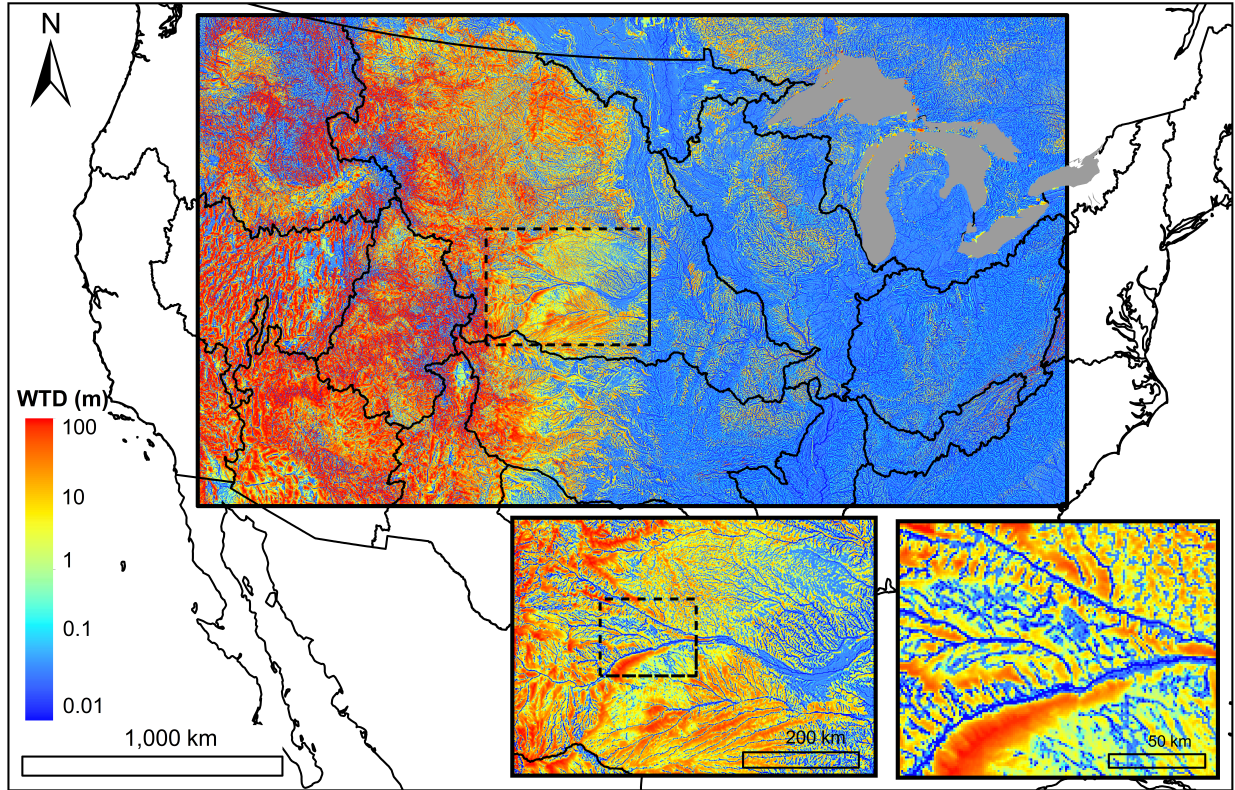


442
443
444

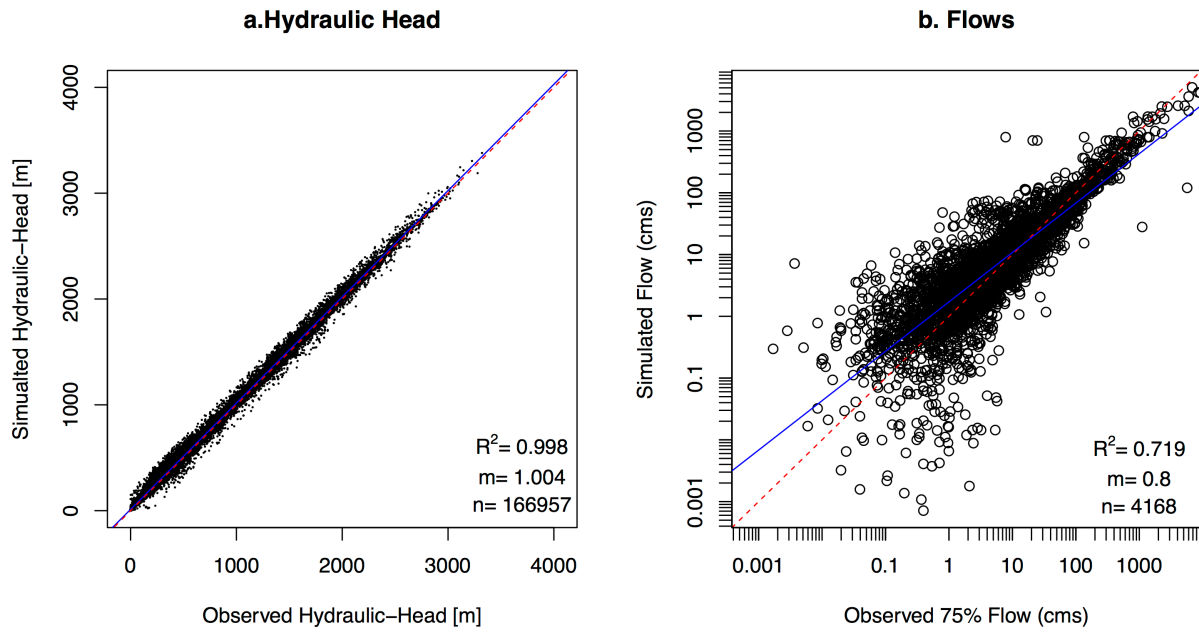
Figure 2. Plot of observed streamflow (a) and observed water table depth (b).



445
 446 Figure 3. Map of simulated surface flow (m^3/s) over the CONUS domain with two insets
 447 zooming into the Ohio river basin. Colors represent surface flow in log scale and line widths
 448 vary slightly with flow for the first two panels.
 449



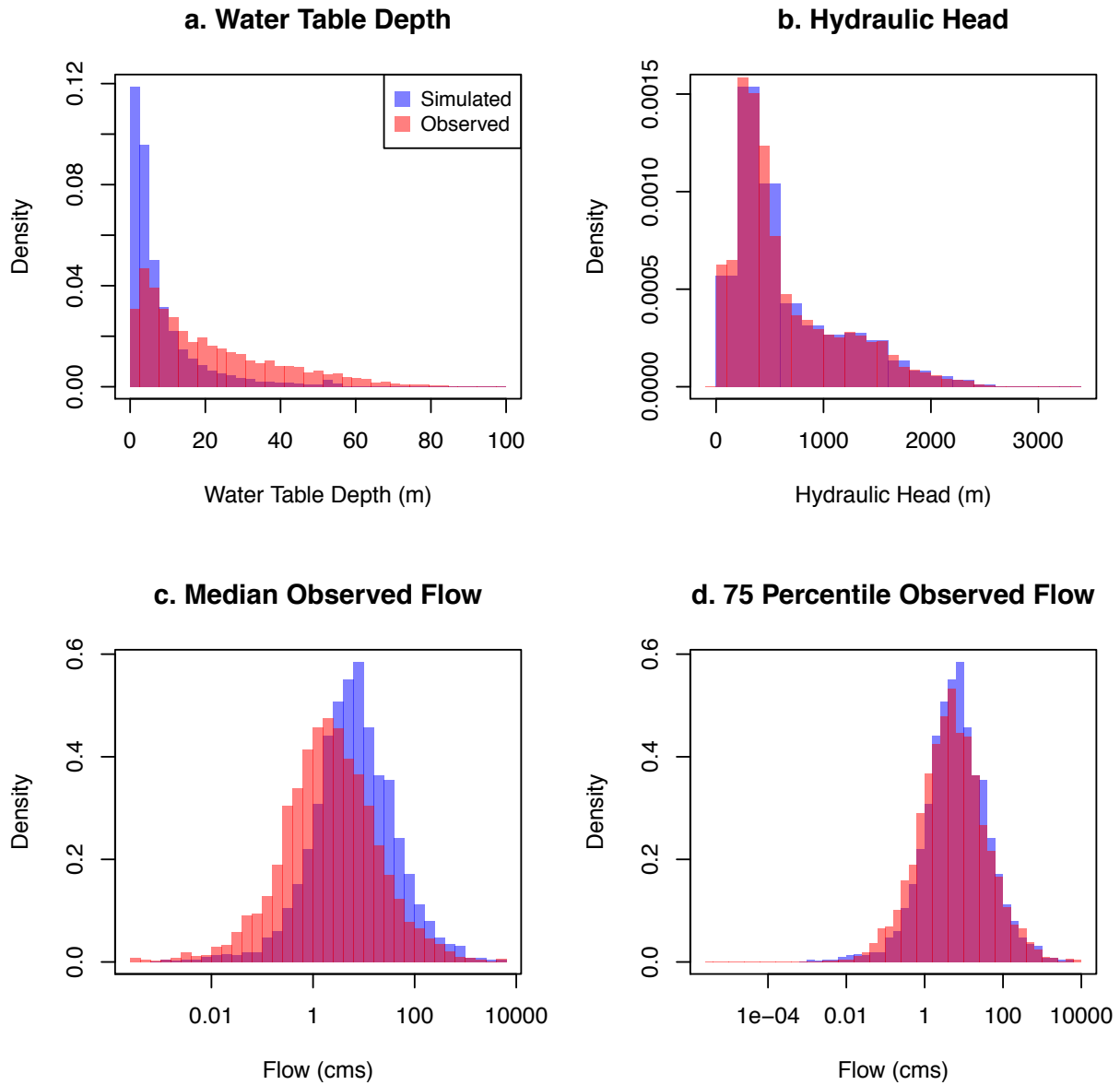
450
451 Figure 4. Map of water table depth (m) over the simulation domain with two insets zooming into
452 the North and South Platte River basin, headwaters to the Mississippi. Colors represent depth in
453 log scale (from 0.01 to 100m).
454



455

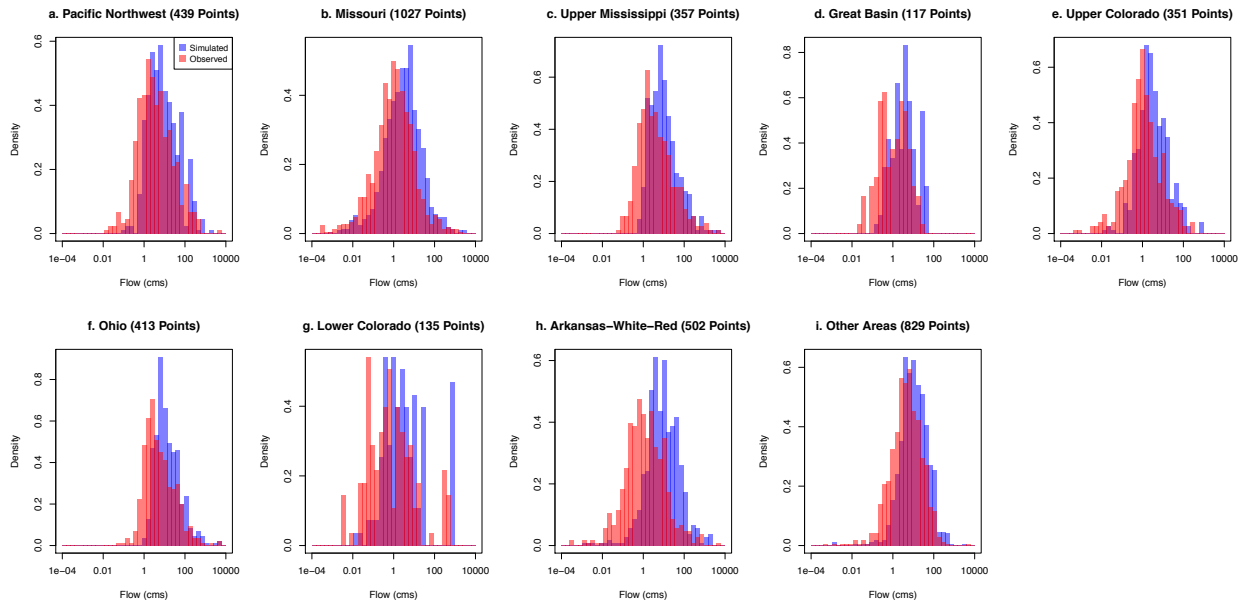
456 Figure 5. Scatterplots of simulated v. observed hydraulic head (a) and surface flow (b).

457



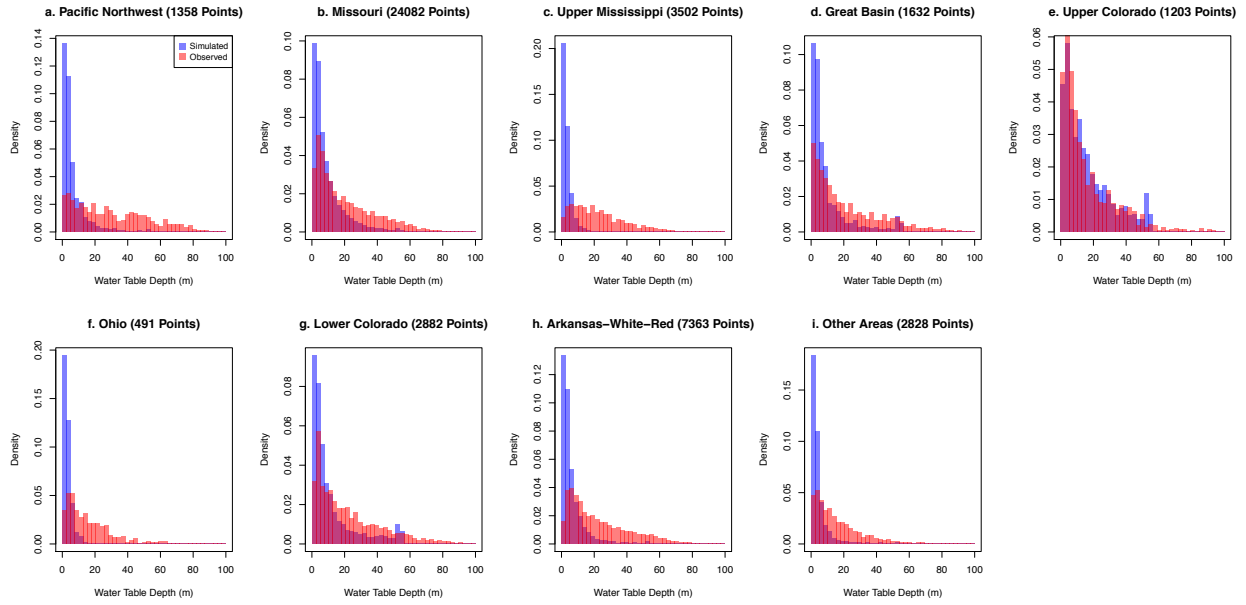
458
 459 Figure 6. Histograms of simulated and observed water table depth (a), hydraulic head (b),
 460 median observed flow (c) and 75th percentile observed flow (d).
 461

462
463



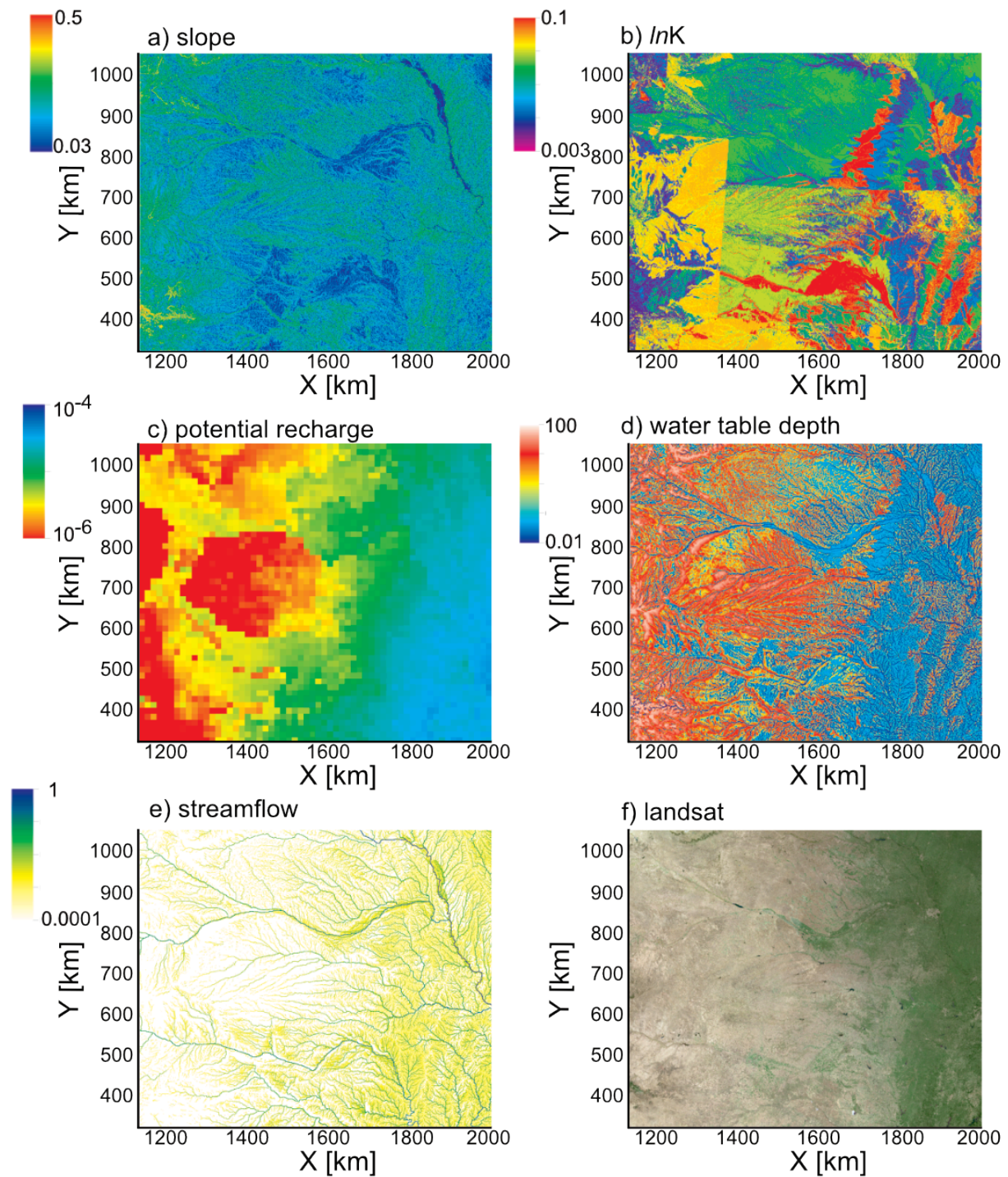
464
465
466

Figure 7. Distributions of observed and simulated streamflow by basin as indicated.

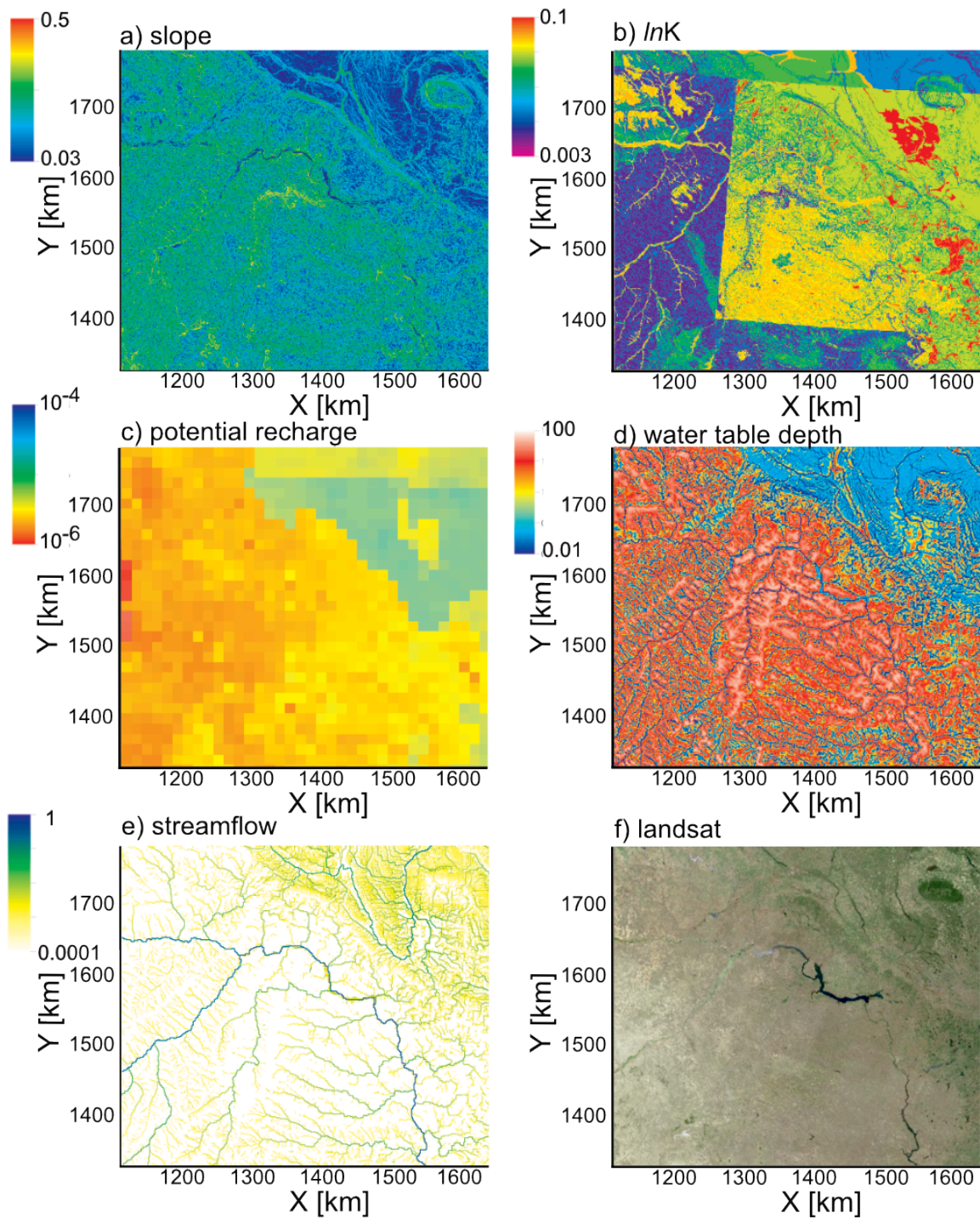


467
468

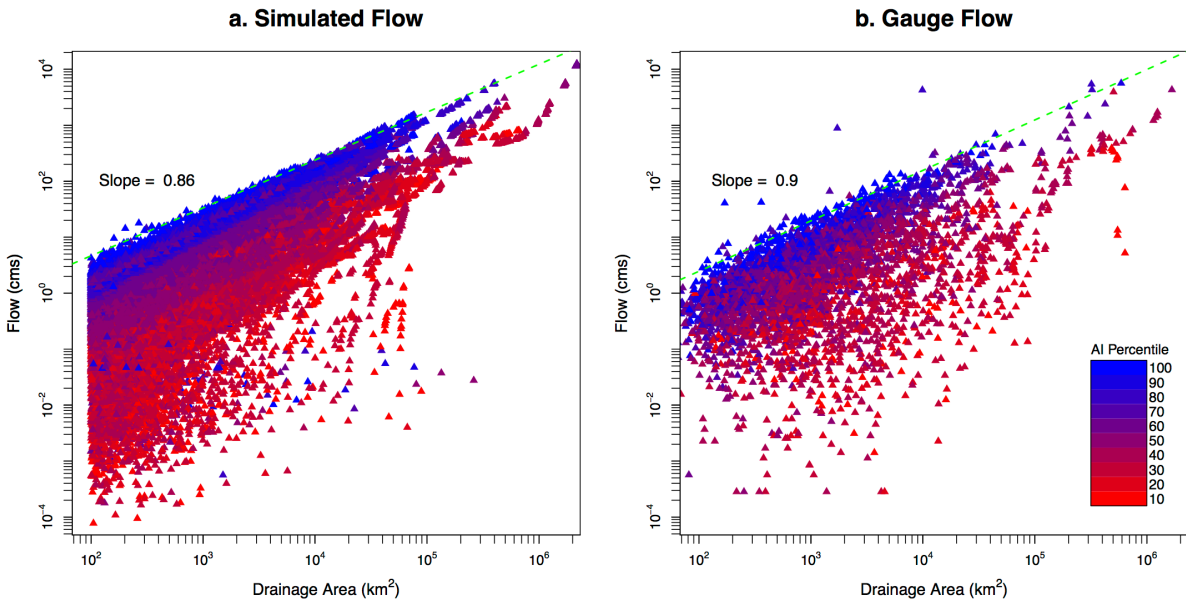
Figure 8. Distributions of observed and simulated water table depth by basin as indicated.



469
 470 Figure 9. Plots of topographic slope (a), hydraulic conductivity (b) potential recharge (c), water
 471 table depth (d), streamflow (e) and satellite image (f) for a region of the model covering the
 472 Platte River basin.
 473



474
 475 Figure 10. Plots of topographic slope (a), hydraulic conductivity (b) potential recharge (c), water
 476 table depth (d), streamflow (e) and satellite image (f) for a region of the model covering the
 477 Upper Missouri basin.



478
 479 Figure 11. Plots of scaling relationships for simulated and median observed surface flow. Log-
 480 scale plots of surface flow as a function of contributing drainage area derived from the model
 481 simulation (a) and observations (b). Individual symbols are colored by aridity index (AI) with
 482 blue colors being humid and red colors being arid in panels (a) and (b).
 483
 484
 485

486
487
488
489
490
491
492
493
494
495
496
497
498
499
500
501
502
503
504
505
506
507
508
509
510
511
512
513
514
515
516
517
518
519
520
521
522
523
524
525
526
527
528
529
530

References

- Anyah, R. O., C. P. Weaver, G. Miguez-Macho, Y. Fan and A. Robock (2008). "Incorporating water table dynamics in climate modeling: 3. Simulated groundwater influence on coupled land-atmosphere variability." Journal of Geophysical Research-Atmospheres **113**(D7): 15,
- Ashby, S. F. and R. D. Falgout (1996). "A parallel multigrid preconditioned conjugate gradient algorithm for groundwater flow simulations." Nuclear Science and Engineering **124**(1): 145-159,
- Beven, K. (2004). "Robert e. Horton's perceptual model of infiltration processes." Hydrological Processes **18**(17): 3447-3460,
- Bierkens, M. F. P., V. A. Bell, P. Burek, N. Chaney, L. E. Condon, C. H. David, A. de Roo, P. Döll, N. Drost, J. S. Famiglietti, M. Flörke, D. J. Gochis, P. Houser, R. Hut, J. Keune, S. Kollet, R. M. Maxwell, J. T. Reager, L. Samaniego, E. Sudicky, E. H. Sutanudjaja, N. van de Giesen, H. Winsemius and E. F. Wood (2015). "Hyper-resolution global hydrological modelling: What is next?" Hydrological Processes **29**(2): 310-320, 10.1002/hyp.10391
- Camporese, M., C. Paniconi, M. Putti and S. Orlandini (2010). "Surface-subsurface flow modeling with path-based runoff routing, boundary condition-based coupling, and assimilation of multisource observation data." Water Resources Research **46**(2): W02512, 10.1029/2008wr007536
- Camporese, M., C. Paniconi, M. Putti and S. Orlandini (2010). "Surface-subsurface flow modeling with path-based runoff routing, boundary condition-based coupling, and assimilation of multisource observation data." Water Resour. Res. **46**(2): W02512, doi: 10.1029/2008wr007536
- Camporese, M., D. Penna, M. Borga and C. Paniconi (2014). "A field and modeling study of nonlinear storage-discharge dynamics for an alpine headwater catchment." Water Resources Research **50**(2): 806-822, 10.1002/2013wr013604
- Condon, L. E. and R. M. Maxwell (2013). "Implementation of a linear optimization water allocation algorithm into a fully integrated physical hydrology model." Advances in Water Resources **60**(0): 135-147, <http://dx.doi.org/10.1016/j.advwatres.2013.07.012>
- Condon, L. E. and R. M. Maxwell (2014). "Feedbacks between managed irrigation and water availability: Diagnosing temporal and spatial patterns using an integrated hydrologic model." Water Resources Research **50**(3): 2600-2616, 10.1002/2013wr014868
- Condon, L. E., R. M. Maxwell and S. Gangopadhyay (2013). "The impact of subsurface conceptualization on land energy fluxes." Advances in Water Resources **60**(0): 188-203, <http://dx.doi.org/10.1016/j.advwatres.2013.08.001>
- Döll, P., H. Hoffmann-Dobrev, F. T. Portmann, S. Siebert, A. Eicker, M. Rodell, G. Strassberg and B. R. Scanlon (2012). "Impact of water withdrawals from groundwater and surface water on continental water storage variations." - **59**, **160**(- 0): - 156,
- Dunne, T. (1983). "Relation of field studies and modeling in the prediction of storm runoff." Journal of Hydrology **65**(1, 3): 25-48, [http://dx.doi.org/10.1016/0022-1694\(83\)90209-3](http://dx.doi.org/10.1016/0022-1694(83)90209-3)
- Fan, Y., H. Li and G. Miguez-Macho (2013). "Global patterns of groundwater table depth." Science **339**(6122): 940-943, 10.1126/science.1229881

531 Fan, Y., G. Miguez-Macho, C. P. Weaver, R. Walko and A. Robock (2007). "Incorporating
532 water table dynamics in climate modeling: 1. Water table observations and equilibrium
533 water table simulations." Journal of Geophysical Research-Atmospheres **112**(D10): -,
534 Ferguson, I. M. and R. M. Maxwell (2011). "Hydrologic and land–energy feedbacks of
535 agricultural water management practices." Environmental Research Letters - **6**(- 1),
536 doi:10.1088/1748-9326/6/1/014006

537 Ferguson, I. M. and R. M. Maxwell (2012). "Human impacts on terrestrial hydrology: Climate
538 change versus pumping and irrigation." Environmental Research Letters **7**(4): 044022,
539 Freeze, R. A. and R. L. Harlan (1969). "Blueprint for a physically-based, digitally-simulated
540 hydrologic response model." Journal of Hydrology **9**: 237-258,
541 Glaster, J. C. (2009). "Testing the linear relationship between peak annual river discharge and
542 drainage area using long-term usgs river gauging records." Geological Society of
543 America Special Papers **451**: 159-171, 10.1130/2009.2451(11)

544 Gleeson, T. and M. Cardiff (2014). "The return of groundwater quantity: A mega-scale and
545 interdisciplinary “future of hydrogeology”?" Hydrogeology Journal: **4**, 10.1007/s10040-
546 013-0998-8

547 Gleeson, T., L. Marklund, L. Smith and A. H. Manning (2011). "Classifying the water table at
548 regional to continental scales." Geophysical Research Letters **38**(L05401): 6,
549 10.1029/2010GL046427

550 Gleeson, T., L. Smith, N. Moosdorf, J. Hartmann, H. H. Dürr, A. H. Manning, L. P. H. van Beek
551 and A. M. Jellinek (2011). "Mapping permeability over the surface of the earth."
552 Geophysical Research Letters **38**(2): L02401, 10.1029/2010gl045565

553 Goderniaux, P., S. Brouyere, H. J. Fowler, S. Blenkinsop, R. Therrien, P. Orban and A.
554 Dassargues (2009). "Large scale surface, subsurface hydrological model to assess
555 climate change impacts on groundwater reserves." Journal of Hydrology **373**(1, 2):
556 122-138, <http://dx.doi.org/10.1016/j.jhydrol.2009.04.017>

557 Horton, R. E. (1933). "The role of infiltration in the hydrologic cycle." Transactions-American
558 Geophysical Union **14**: 446-460,

559 Jiang, X., G. Y. Niu and Z. L. Yang (2009). "Impacts of vegetation and groundwater dynamics
560 on warm season precipitation over the central united states." Journal of Geophysical
561 Research **114**: 15,

562 Jones, J. E. and C. S. Woodward (2001). "Newton-krylov-multigrid solvers for large-scale,
563 highly heterogeneous, variably saturated flow problems." Advances in Water Resources
564 **24**(7): 763-774,

565 Jones, J. P., E. A. Sudicky, A. E. Brookfield and Y. J. Park (2006). "An assessment of the tracer-
566 based approach to quantifying groundwater contributions to streamflow." Water Resour.
567 Res. **42**, 10.1029/2005wr004130

568 Jones, J. P., E. A. Sudicky and R. G. McLaren (2008). "Application of a fully-integrated surface-
569 subsurface flow model at the watershed-scale: A case study." Water Resources Research
570 **44**(3): W03407, 10.1029/2006wr005603

571 Justice, C. O., J. R. G. Townshend, E. F. Vermote, E. Masuoka, R. E. Wolfe, N. Saleous, D. P.
572 Roy and J. T. Morisette (2002). "An overview of modis land data processing and product
573 status." Remote Sensing of Environment **83**(1, 2): 3-15,
574 [http://dx.doi.org/10.1016/S0034-4257\(02\)00084-6](http://dx.doi.org/10.1016/S0034-4257(02)00084-6)

575 Kirkby, M. (1988). "Hillslope runoff processes and models." Journal of Hydrology **100**(1, 3):
576 315-339, [http://dx.doi.org/10.1016/0022-1694\(88\)90190-4](http://dx.doi.org/10.1016/0022-1694(88)90190-4)

577 Kollet, S. J. (2009). "Influence of soil heterogeneity on evapotranspiration under shallow water
578 table conditions: Transient, stochastic simulations." Environmental Research Letters **4**(3):
579 9,

580 Kollet, S. J., I. Cvijanovic, D. Schüttemeyer, R. M. Maxwell, A. F. Moene and B. P. (2009).
581 "The influence of rain sensible heat, subsurface heat convection and the lower
582 temperature boundary condition on the energy balance at the land surface." Vadose Zone
583 Journal **8**(4): 12,

584 Kollet, S. J. and R. M. Maxwell (2006). "Integrated surface-groundwater flow modeling: A free-
585 surface overland flow boundary condition in a parallel groundwater flow model." Advances in
586 Water Resources **29**(7): 945-958,

587 Kollet, S. J. and R. M. Maxwell (2008). "Capturing the influence of groundwater dynamics on
588 land surface processes using an integrated, distributed watershed model." Water
589 Resources Research **44**(W02402): 18, doi:10.1029/2007WR006004

590 Kollet, S. J., R. M. Maxwell, C. S. Woodward, S. Smith, J. Vanderborght, H. Vereecken and C.
591 Simmer (2010). "Proof of concept of regional scale hydrologic simulations at hydrologic
592 resolution utilizing massively parallel computer resources." Water Resources Research
593 **46**(W04201): -, Doi 10.1029/2009wr008730

594 Krakauer, N. Y., H. Li and Y. Fan (2014). "Groundwater flow across spatial scales: Importance
595 for climate modeling." Environmental Research Letters **9**(3): 034003,

596 Kumar, M., C. J. Duffy and K. M. Salvage (2009). "A second order accurate, finite volume
597 based, integrated hydrologic modeling (fihm) framework for simulation of surface and
598 subsurface flow." Vadose Zone Journal,

599 Maurer, E. P., A. W. Wood, J. C. Adam, D. P. Lettenmaier and B. Nijssen (2002). "A long-term
600 hydrologically based dataset of land surface fluxes and states for the conterminous united
601 states*." Journal of Climate **15**(22): 3237-3251, 10.1175/1520-
602 0442(2002)015<3237:althbd>2.0.co;2

603 Maxwell, R. M. (2013). "A terrain-following grid transform and preconditioner for parallel,
604 large-scale, integrated hydrologic modeling." Advances in Water Resources **53**: 109-117,
605 <http://dx.doi.org/10.1016/j.advwatres.2012.10.001>

606 Maxwell, R. M., F. K. Chow and S. J. Kollet (2007). "The groundwater-land-surface-atmosphere
607 connection: Soil moisture effects on the atmospheric boundary layer in fully-coupled
608 simulations." Advances in Water Resources **30**(12): 2447-2466, Doi
609 10.1016/J.Advwatres.2007.05.018

610 Maxwell, R. M. and S. J. Kollet (2008). "Interdependence of groundwater dynamics and land-
611 energy feedbacks under climate change." Nature Geosci **1**(10): 665-669,

612 Maxwell, R. M. and S. J. Kollet (2008). "Quantifying the effects of three-dimensional subsurface
613 heterogeneity on hortonian runoff processes using a coupled numerical, stochastic
614 approach." Advances in Water Resources **31**(5): 807-817,

615 Maxwell, R. M., J. D. Lundquist, J. D. Mirocha, S. G. Smith, C. S. Woodward and A. F. B.
616 Tompson (2011). "Development of a coupled groundwater-atmospheric model." Monthly
617 Weather Review doi: **10.1175/2010MWR3392**(139): 96-116,

618 Maxwell, R. M., M. Putti, S. Meyerhoff, J.-O. Delfs, I. M. Ferguson, V. Ivanov, J. Kim, O.
619 Kolditz, S. J. Kollet, M. Kumar, S. Lopez, J. Niu, C. Paniconi, Y.-J. Park, M. S.
620 Phanikumar, C. Shen, E. A. Sudicky and M. Sulis (2014). "Surface-subsurface model
621 intercomparison: A first set of benchmark results to diagnose integrated hydrology and
622 feedbacks." Water Resources Research **50**(2): 1531-1549, 10.1002/2013wr013725

623 Miguez-Macho, G., Y. Fan, C. P. Weaver, R. Walko and A. Robock (2007). "Incorporating
624 water table dynamics in climate modeling: 2. Formulation, validation, and soil moisture
625 simulation." *Journal of Geophysical Research-Atmospheres* **112**(D13): -,
626 Mikkelsen, K. M., R. M. Maxwell, I. Ferguson, J. D. Stednick, J. E. McCray and J. O. Sharp
627 (2013). "Mountain pine beetle infestation impacts: Modeling water and energy budgets at
628 the hill-slope scale." *Ecohydrology* **6**(1): 64-72, 10.1002/eco.278
629 Osei-Kuffuor, D., R. M. Maxwell and C. S. Woodward "Improved numerical solvers for implicit
630 coupling of subsurface and overland flow." *Advances in Water Resources*(0),
631 <http://dx.doi.org/10.1016/j.advwatres.2014.09.006>
632 Osei-Kuffuor, D., R. M. Maxwell and C. S. Woodward (2014). "Improved numerical solvers for
633 implicit coupling of subsurface and overland flow." *Advances in Water Resources* **74**(0):
634 185-195, <http://dx.doi.org/10.1016/j.advwatres.2014.09.006>
635 Qu, Y. and C. J. Duffy (2007). "A semidiscrete finite volume formulation for multiprocess
636 watershed simulation." *Water Resources Research* **43**(W08419): 18,
637 doi:10.1029/2006WR005752
638 Richards, L. A. (1931). "Capillary conduction of liquids in porous mediums." *Physics* **1**: 318-
639 333,
640 Rihani, J. F., R. M. Maxwell and F. K. Chow (2010). "Coupling groundwater and land surface
641 processes: Idealized simulations to identify effects of terrain and subsurface
642 heterogeneity on land surface energy fluxes." *Water Resour. Res.* **46**: 1-14,
643 doi:10.1029/2010WR009111
644 Rodell, M., I. Velicogna and J. S. Famiglietti (2009). "Satellite-based estimates of groundwater
645 depletion in india." *Nature* **460**(7258): 999-1002,
646 Rodriguez-Iturbe, I. and A. Rinaldo (2001). *Fractal river basins: Chance and self-organization*,
647 Cambridge University Press.
648 Schaap, M. G. and F. J. Leij (1998). "Database-related accuracy and uncertainty of pedotransfer
649 functions." *Soil Science* **163**(10): 765-779,
650 Shi, Y., K. J. Davis, C. J. Duffy and X. Yu (2013). "Development of a coupled land surface
651 hydrologic model and evaluation at a critical zone observatory." *Journal of*
652 *Hydrometeorology* **14**(5): 1401-1420, 10.1175/jhm-d-12-0145.1
653 Sudicky, E., J. Jones, Y.-J. Park, A. Brookfield and D. Colautti (2008). "Simulating complex
654 flow and transport dynamics in an integrated surface-subsurface modeling framework."
655 *Geosciences Journal* **12**(2): 107-122, 10.1007/s12303-008-0013-x
656 Sulis, M., C. Paniconi, M. Marrocu, D. Huard and D. Chaumont (2012). "Hydrologic response to
657 multimodel climate output using a physically based model of groundwater/surface water
658 interactions." *Water Resources Research* **48**(12): W12510, 10.1029/2012wr012304
659 Taylor, R. G., B. Scanlon, P. Doll, M. Rodell, R. van Beek, Y. Wada, L. Longuevergne, M.
660 Leblanc, J. S. Famiglietti, M. Edmunds, L. Konikow, T. R. Green, J. Chen, M. Taniguchi,
661 M. F. P. Bierkens, A. MacDonald, Y. Fan, R. M. Maxwell, Y. Yechieli, J. J. Gurdak, D.
662 M. Allen, M. Shamsudduha, K. Hiscock, P. J. F. Yeh, I. Holman and H. Treidel (2013).
663 "Ground water and climate change." *Nature Clim. Change* **3**(4): 322-329,
664 Therrien, R., E. Sudicky, Y. Park and R. McLaren (2012). *Hydrogeosphere: A three-dimensional*
665 *numerical modelling describing fully-*
666 *integrated subsurface and surface flow and transport. User guide. Waterloo, Ontario, Canada,*
667 *Aquanty Inc.*

668 van Genuchten, M. T. (1980). "A closed-form equation for predicting the hydraulic conductivity
669 of unsaturated soils." Soil Science Society of America Journal **44**(5): 892-898,
670 VanderKwaak, J. E. and K. Loague (2001). "Hydrologic-response simulations for the r-5
671 catchment with a comprehensive physics-based model." Water Resources Research
672 **37**(4): 999-1013,
673 Williams, J. L. and R. M. Maxwell (2011). "Propagating subsurface uncertainty to the
674 atmosphere using fully-coupled, stochastic simulations." Journal of Hydrometeorology,
675 doi:10.1175/2011JHM1363.1
676 Wood, B. D. (2009). "The role of scaling laws in upscaling." Advances in Water Resources
677 **32**(5): 723-736, <http://dx.doi.org/10.1016/j.advwatres.2008.08.015>
678 Wood, E. F., J. K. Roundy, T. J. Troy, L. P. H. van Beek, M. F. P. Bierkens, E. Blyth, A. de Roo,
679 P. Döll, M. Ek, J. Famiglietti, D. Gochis, N. van de Giesen, P. Houser, P. R. Jaffé, S.
680 Kollet, B. Lehner, D. P. Lettenmaier, C. Peters-Lidard, M. Sivapalan, J. Sheffield, A.
681 Wade and P. Whitehead (2011). "Hyperresolution global land surface modeling: Meeting
682 a grand challenge for monitoring earth's terrestrial water." Water Resources Research
683 **47**(5): W05301, 10.1029/2010wr010090
684 Xia, Y., K. Mitchell, M. Ek, B. Cosgrove, J. Sheffield, L. Luo, C. Alonge, H. Wei, J. Meng, B.
685 Livneh, Q. Duan and D. Lohmann (2012). "Continental-scale water and energy flux
686 analysis and validation for north american land data assimilation system project phase 2
687 (nldas-2): 2. Validation of model-simulated streamflow." Journal of Geophysical
688 Research: Atmospheres **117**(D3): D03110, 10.1029/2011jd016051
689
690